Supplementary Materials

Supplementary Methods

CT Image Acquisition Protocol

Patients were instructed to fast for at least 6 h prior to the scan. To reduce gastric motility artifacts, 10 mg Anisodamine (654-2) was administered via intramuscular injection approximately 10 min before scanning. Optimal gastric distension was achieved by oral ingestion of 800–1000 mL of water or 6 g of effervescent granules immediately prior to the scan. The scan coverage was extended craniocaudally from the dome of the diaphragm to the pubic symphysis. The protocol commenced with an initial unenhanced scan acquired using a tube voltage of 120 kVp, an effective tube current-time product of 210 mAs, detector collimation of 128 × 0.6 mm, and a pitch of 0.9. Subsequently, contrast-enhanced scans were performed in dual-energy mode following intravenous administration of a non-ionic iodinated contrast medium (Iohexol, 350 mg I/mL; GE Healthcare, China) via the antecubital vein using a power injector at a rate of 3.0 mL/s, with the total volume based on patient body weight (2 mL/kg).

Dual-energy acquisitions were obtained during the arterial phase (AP) and the portal venous phase (VP), with scan delays of 25 seconds and 70 seconds post-injection initiation, respectively. The specific DECT parameters included Tube A operating at 100 kVp / 230 ref mAs and Tube B at Sn140 kVp (140 kVp with Tin filtration) / 178 ref mAs, with automatic tube current modulation (Care Dose 4D) enabled. For these dual-energy scans, the detector collimation was set to 32 × 0.6 mm and the pitch was 0.55. While raw data were initially reconstructed into 5 mm thick axial images for diagnostic review, thin-slice axial reconstructions with a 1 mm thickness and 1 mm interval were generated specifically for the subsequent radiomic analysis.

CT Feature Definitions

Clinical T (cT) and N (cN) stages were determined according to the Chinese Society of Clinical Oncology (CSCO) Guidelines for Gastric Cancer (2024

Edition).

a. Tumor Location: Cardia, Gastric body, Gastric antrum, Pylorus.
b. Tumor Morphology: Localized type (Borrmann type I: polypoid; Borrmann type II: localized ulcerative), Infiltrative type (Borrmann type III: infiltrative ulcerative; Borrmann type IV: diffuse infiltrative)
c. Tumor Thickness: Maximum tumor thickness measured perpendicular to the gastric wall.
d. Tumor Enhancement Pattern: Homogeneous enhancement (Difference between maximum and minimum CT values in the venous phase < 10 HU), Inhomogeneous enhancement (Difference between maximum and minimum CT values in the venous phase ≥ 10 HU)
e. Degree of Tumor Enhancement: Obvious enhancement (Net increase in CT value in the venous phase ≥ 40 HU), Not obvious enhancement (Net increase in CT value in the venous phase < 40 HU)
f. cT Stage: cT4 vs. non-cT4 (cT2-3).
g. cN Stage: cN-negative (cN0) vs. cN-positive (cN1-3).

Clinical Data Collection

Relevant clinical data for all enrolled patients were retrospectively collected by reviewing institutional electronic medical records and picture archiving and communication systems (PACS). This information included patient demographics, such as age at surgery and sex, presence of major comorbidities (recorded dichotomously based on medical history), Body Mass Index (BMI, calculated as kg/m^2 and categorized using standard thresholds), and preoperative serum levels of key tumor markers, including carcinoembryonic antigen (CEA), carbohydrate antigen 19-9 (CA19-9), and carbohydrate antigen 72-4 (CA72-4), which were categorized as 'normal' or 'elevated' according to our institution.

Radiomics Workflow

The 1-mm thick axial venous phase DECT datasets were imported to a

dedicated image-processing workstation (SyngoMMWP, VE36A; Siemens Healthineers, Germany). Using the integrated dual-energy analysis software application (Liver VNC mode), iodine maps quantitatively representing iodine concentration were generated from the DECT data. For the radiomics analysis, performed using the Siemens Frontier research platform (Siemens Healthineers), two sets of 1-mm thick images were utilized: (1) linearly blended images, simulating conventional 120-kVp acquisition (referred to as 'blended images'), and (2) the corresponding derived IM. Tumor segmentation was performed manually on the blended images by Observer 1, referencing the corresponding coronal and sagittal planes to ensure accurate three-dimensional delineation. The entire gross tumor volume was contoured slice-by-slice along its visible margins, meticulously excluding adjacent non-tumor structures, such as perigastric fat, major blood vessels, and intraluminal contents (air/fluid), thereby defining the volume of interest (VOI) (Fig.1A). This primary VOI mask, generated on the blended image, was then automatically co-registered and applied to the corresponding iodine map dataset to ensure that identical spatial regions were analyzed for both image types.

Radiomic Feature Extraction and Preprocessing

All features, compliant with Image Biomarker Standardization Initiative (IBSI) definitions where applicable, included: (a) First-order statistics (histogram analysis describing the distribution of voxel intensities), (b) Shape-based features (characterizing the 3D size and geometry of the VOI), and (c) Texture features quantifying tumor heterogeneity using matrices such as Gray Level Co-occurrence Matrix (GLCM), Gray Level Run Length Matrix (GLRLM), Gray Level Size Zone Matrix (GLSZM), Gray Level Dependence Matrix (GLDM), and Neighborhood Gray Tone Difference Matrix (NGTDM). Prior to texture feature calculation, image intensities within the VOI were typically discretized using a fixed bin number of 25. All extracted features subsequently underwent z-score normalization based on the feature distributions within the training set.

Supplementary Results

A total of 1691 features were extracted from the iodine maps and the blended images, respectively. From the original (unfiltered) images of each type, 110 features were extracted, categorized as follows: 3D Shape features (n=17); First-order Statistics features (n=18); Texture features (n=75), including: Gray Level Co-occurrence Matrix (GLCM, n=24), Gray Level Run Length Matrix (GLRLM, n=16), Gray Level Size Zone Matrix (GLSZM, n=16), Gray Level Dependence Matrix (GLDM, n=14), Neighboring Gray Tone Difference Matrix (NGTDM, n=5). An additional 1581 features were extracted from images derived after applying the filtering and transformation steps described in the preprocessing section. The stability of the clinical-radiomics model was supported by an adequate events per variable (EPV) ratio (>10) in the training set (43 events / 4 variables).

Patient-specific risk scores for predicting DFS and OS were calculated using the coefficients from the respective final clinical-radiomics models:

DFS Risk Score = 2.365 × Rad-score + 1.121 × Morphology + 0.746 × CEA + 0.651 × cN stage

OS Risk Score = 3.486 × Rad-score + 0.925 × CEA + 0.793 × Morphology + 0.755 × cN stage

Supplementary Table 1 Clinical Information of Patients in Training and Validation Sets

Variables	Training Set (n=122)	Validation Set (n=53)	*P* value
Gender			1.000
Female	21 (17.2%)	9 (17.0%)	
Male	101 (82.8%)	44 (83.0%)	
Age (years)			0.772
<60	53 (43.4%)	25 (47.2%)	
≥60	69 (56.6%)	28 (52.8%)	
Comorbidities			0.243
No	65 (53.3%)	34 (64.2%)	
Yes	57 (46.7%)	19 (35.8%)	
BMI			0.781[b]
<18.5	8 (6.56%)	4 (7.55%)	
18.5-24.0	67 (54.9%)	26 (49.1%)	
≥24.0	47 (38.5%)	23 (43.4%)	
CEA			0.572
Normal	94 (77.0%)	38 (71.7%)	
Elevated	28 (23.0%)	15 (28.3%)	
CA19-9			0.687
Normal	94 (77.0%)	43 (81.1%)	
Elevated	28 (23.0%)	10 (18.9%)	
CA72-4			0.360
Normal	101 (82.8%)	40 (75.5%)	
Elevated	21 (17.2%)	13 (24.5%)	
Tumor location			0.131[b]
Cardia	27 (22.1%)	20 (37.7%)	
Gastric body	43 (35.2%)	19 (35.8%)	
Gastric antrum	39 (32.0%)	11 (20.8%)	

Pylorus	13 (10.7%)	3 (5.66%)	
Tumor morphology			1.000
Localized	26 (21.3%)	11 (20.8%)	
Infiltrative	96 (78.7%)	42 (79.2%)	
Tumor thickness (cm)	1.43 [1.05;1.73]	1.37 [1.09;1.74]	0.766[a]
Enhancement pattern			1.000
Inhomogeneous	61 (50.0%)	26 (49.1%)	
Homogeneous	61 (50.0%)	27 (50.9%)	
Enhancement degree			1.000
No obvious	33 (27.0%)	14 (26.4%)	
Obvious	89 (73.0%)	39 (73.6%)	
cT stage			0.388
Non-cT4	27 (22.1%)	8 (15.1%)	
cT4	95 (77.9%)	45 (84.9%)	
cN stage			0.239
Negative	35 (28.7%)	10 (18.9%)	
Positive	87 (71.3%)	43 (81.1%)	
pT stage			0.206
T2	17 (13.9%)	9 (17.0%)	
T3	7 (5.74%)	0 (0.00%)	
T4	98 (80.3%)	44 (83.0%)	
pN stage			0.925
N0	27 (22.1%)	12 (22.6%)	
N1	30 (24.6%)	11 (20.8%)	
N2	34 (27.9%)	17 (32.1%)	
N3	31 (25.4%)	13 (24.5%)	
Recurrence or			0.278

metastasis			
No	79 (64.8%)	29 (54.7%)	
Yes	43 (35.2%)	24 (45.3%)	
Survival status			0.107
Alive	86 (70.5%)	30 (56.6%)	
Dead	36 (29.5%)	23 (43.4%)	

Tumor thickness was presented as median with interquartile range, otherwise in parentheses with percentages. [a] p value derived from the Wilcoxon rank-sum test; [b] p value derived from the Fisher's exact test, the other p value was from the Pearson's chi-square test.

Supplementary Table 2 Univariate and Multivariate Cox Regression Analyses for Patients in the Training Set

Variables	Univariate Analysis		Multivariate Analysis	
	HR (95% CI)	*P* value	HR (95% CI)	*P* value
CEA	2.222(1.184-4.168)	0.013	2.317(1.231-4.362)	0.009
CA19-9	1.939(1.024-3.674)	0.042		
Tumor morphology	4.438(1.372-14.356)	0.013	3.696(1.128-12.105)	0.031
Tumor thickness	1.720(1.175-2.518)	0.005		
cN stage	3.863(1.519-9.821)	0.005	3.027(1.181-7.757)	0.021

Supplementary Table 3 Nine Radiomics Features and Their Coefficients

Feature Name	Coefficient
square_firstorder_Energy	0.050666626
wavelet-HHH_firstorder_Energy	0.018696239
wavelet-HHL_firstorder_Energy	0.005266219
wavelet-HLL_firstorder_Energy	0.072481438
IOwavelet-HLH_glszm_SmallAreaLowGrayLevelEmphasis	-0.088431602
IOwavelet-HLL_glszm_SizeZoneNonUniformity	0.016832783
IOwavelet-LHH_glszm_SizeZoneNonUniformity	0.037792651
IOwavelet-LHL_glszm_LargeAreaHighGrayLevelEmphasis	0.062867260
IOlog-sigma-3-5-mm-3D_gldm_DependenceVariance	-0.022353863

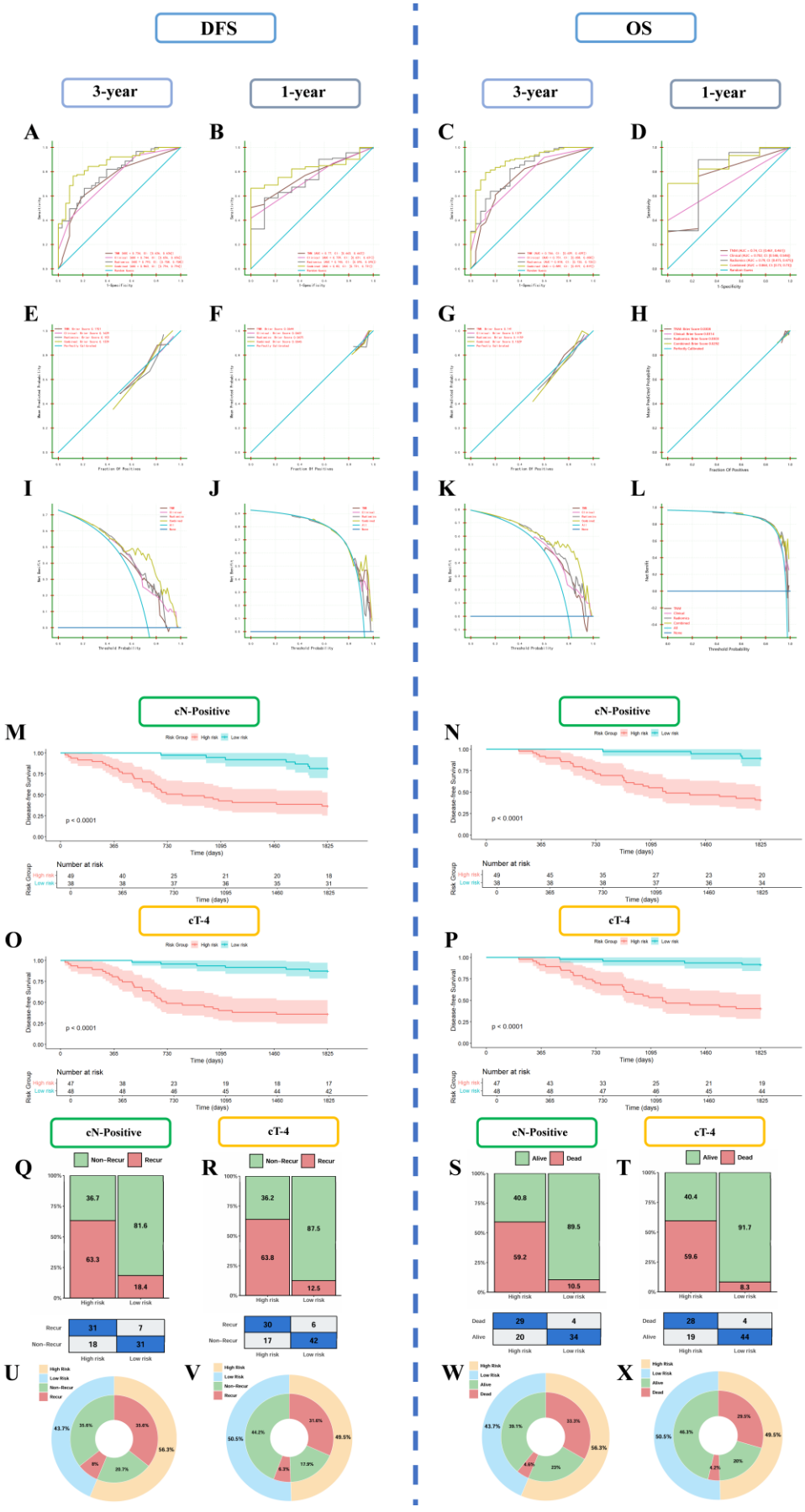
*Radiomics features with the IO prefix are extracted from iodine maps.

Supplementary Table 4 Comparison of Model Performance

Model 1	Model 2	Train			Validation		
		Model 1 C-index (95%CI)	Model 2 C-index (95%CI)	*P* value	Model 1 C-index (95%CI)	Model 2 C-index (95%CI)	*P* value
DFS							
Clinical-Radiomics	Clinical	0.771 (0.713-0.830)	0.693 (0.625-0.761)	0.007	0.712 (0.615-0.809)	0.677 (0.582-0.772)	0.029
Clinical-Radiomics	Radiomics	0.771 (0.713-0.830)	0.708 (0.637-0.779)	0.023	0.712 (0.615-0.809)	0.642 (0.538-0.746)	0.189
Clinical-Radiomics	pTNM	0.771 (0.713-0.830)	0.686 (0.612-0.759)	0.020	0.712 (0.615-0.809)	0.665 (0.550-0.779)	0.360
OS							
Clinical-Radiomics	Clinical	0.821 (0.757-0.884)	0.696 (0.621-0.771)	<0.001	0.714 (0.616-0.812)	0.688 (0.593-0.783)	0.142
Clinical-Radiomics	Radiomics	0.821 (0.757-0.884)	0.758 (0.683-0.834)	0.016	0.714 (0.616-0.812)	0.621 (0.510-0.732)	0.109
Clinical-Radiomics	pTNM	0.821 (0.757-0.884)	0.695 (0.612-0.778)	0.003	0.714 (0.616-0.812)	0.689 (0.581-0.797)	0.649

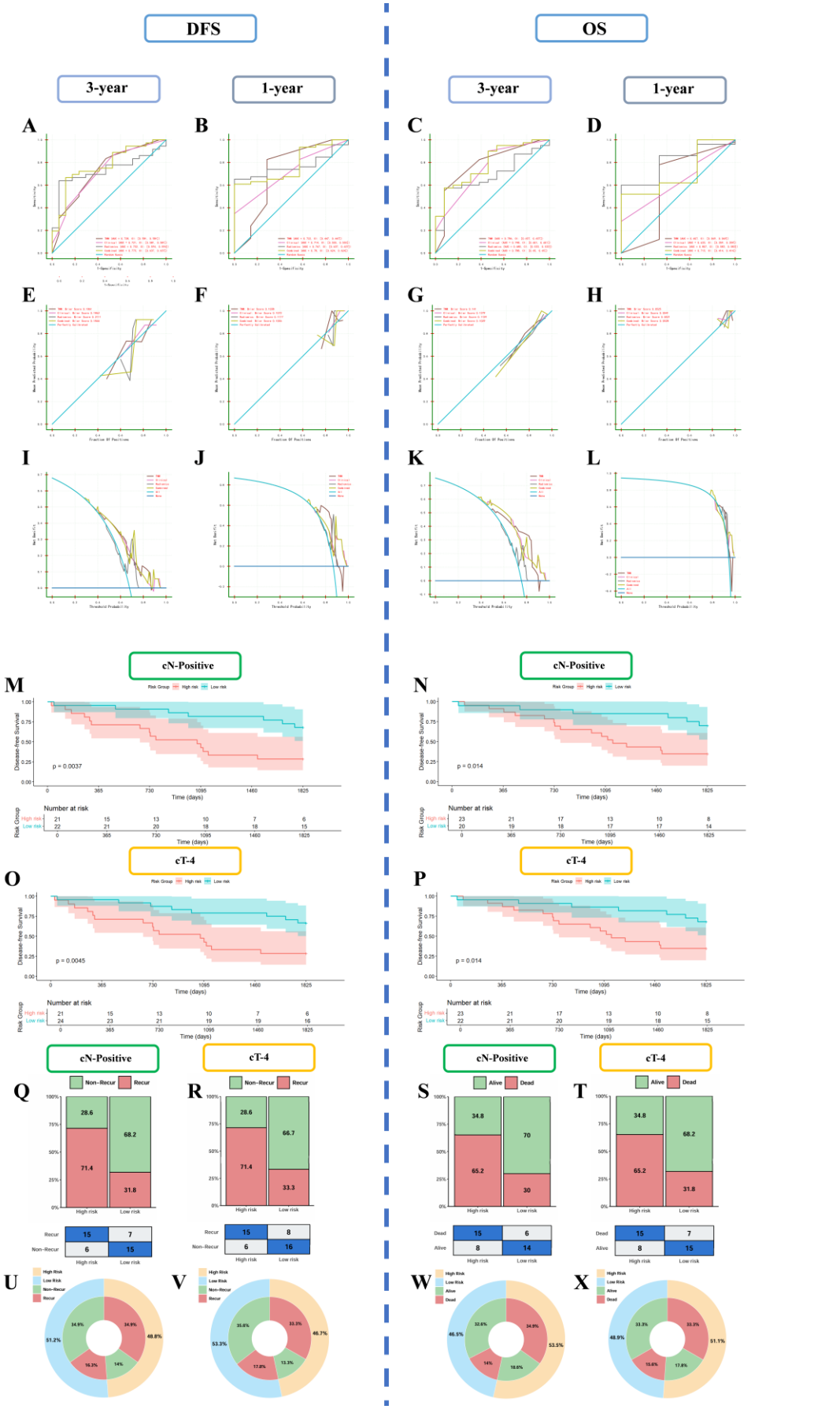
Supplementary Table 5 Model Fit Comparison (AIC)

Model	DFS		OS	
	Train	Validation	Train	Validation
Clinical-Radiomics	366.772	174.623	294.695	166.967
Radiomics	373.839	178.847	300.253	172.220
Clinical	379.452	172.945	318.703	165.222
pTNM	386.009	177.104	327.386	168.696



Supplementary Figure 1 Performance Evaluation of Prognostic Models in the

Training Set. A-L: Comprehensive performance evaluation for 1- and 3-year DFS and OS prediction, including ROC curves, calibration curves, and DCA. M–P: KM curves of high/low-risk subgroups (cN-positive and cT-4 patients). Q–X: Confusion matrices and concentric circle plots showing the classification performance and clinical applicability of the combined model in patients with cT-4 and cN-positive status.



Supplementary Figure 2 Performance Evaluation of Prognostic Models in the

Validation Set. A-L: Comprehensive performance evaluation for 1- and 3-year DFS and OS prediction, including ROC curves, calibration curves, and DCA. M–P: KM curves of high/low-risk subgroups (cN-positive and cT-4 patients). Q–X: Confusion matrices and concentric circle plots showing the classification performance and clinical applicability of the combined model in patients with cT-4 and cN-positive status.